Measurement of Ultrasonic Forces for Particle–Liquid Separations

Steven M. Woodside, Bruce D. Bowen, and James M. Piret
Dept. of Chemical and Bio-Resource Engineering, University of British Columbia, Vancouver, BC, Canada V6T 1Z4

The magnitude and direction of the ultrasonic radiation forces that act on individual particles in a standing-wave field were determined using a microscope-based imaging system. The forces are calculated from measured particle velocities assuming that the drag force, given by Stokes' law, is exactly counterbalanced by the imposed ultrasonic forces. The axial primary radiation force was found to vary sinusoidally with axial position and to be proportional to the local acoustic energy density, as predicted by theory. The magnitude of the transverse primary force was determined by two independent methods to be about 100-fold weaker than the axial force. Separation concepts exploiting the transverse force for cell retention have been successful despite the great disparity in magnitude between the axial and transverse-force components. This may be explained by the reduced hydrodynamic forces on aggregated particles in transverse flow due to their alignment in the sound field.

Introduction

The search for novel solutions to particle-liquid separation problems has engendered a renewed interest in systems that exploit the acoustic forces on particles suspended in a standing ultrasonic wave field. Such systems are distinguished by the fact that they require no physical barrier for separation and no chemical flocculants to enhance aggregation and sedimentation. Although the aggregation of particles in ultrasonic standing waves was first observed more than a century ago (Kundt and Lehmann, 1874), most practical applications and implementations have only recently been identified. A pseudo-standing-wave resonator using modulated ultrasound (Whitworth et al., 1991) and a drifting-field resonator (Benes et al., 1991) were designed to concentrate solid particles by driving them to one end of a chamber. In the inclined resonator of Frank et al. (1993), the flow and ultrasonic fields were oriented such that polystyrene particles were swept to one side of the fluid stream. Ultrasonic standing-wave fields, combined with flow fields, have been exploited to fractionate model polystyrene particles based on size (Mandralis and Feke, 1993a,b; Johnson and Feke, 1995), and to separate different types of polymers based on compressibility (Gupta et al., 1995). The ultrasonic separation of mammalian cells has been successfully used for cell retention in long-term perfusion processes without deleterious effect on the cells (Trampler et al., 1994; Doblhoff-Dier et al., 1994; Pui et al., 1995). The continued rational design of these systems depends on a detailed experimental and theoretical understanding of the ultrasonic forces on particles in a standing-wave field. The relevant ultrasonic forces are the axial and transverse components of the primary radiation force (PRF), and the secondary radiation force (SRF).

Experimental investigations by Higashitani et al. (1981) demonstrated that the transient particle concentration at a pressure antinode plane measured by laser-light absorbance agreed with predictions based on a model that included the axial PRF, fluid drag, and diffusion. Experimentally observed steady-state particle aggregation loci were predicted under different conditions by a model incorporating the axial and transverse PRF, and gravity (Whitworth and Coakley, 1992). The predicted steady-state shape of red blood cell aggregates, formed under the influence of the axial PRF, the SRF, and gravity, have been compared to experimentally observed structures (Weiser et al., 1984).

Correspondence concerning this article should be addressed to J. M. Piret.
Additional address for S. M. Woodside and J. M. Piret: Biotechnology Laboratory, University of British Columbia, Vancouver, BC, Canada V6T 1Z3.

None of the aforementioned studies has experimentally determined the spatial distribution of the ultrasonic forces, nor have they examined thoroughly the relative magnitudes of the various ultrasonic forces and other body and interparticle forces. This information is critical to a practicable model of particle aggregation and for predicting potential separation performance. In this article, a versatile method is presented for the experimental measurement of the acoustic forces on single particles as a function of their position in the field. Through measurements of particle motion in orthogonal planes, the axial and transverse components of the PRF were determined independently.

Background

A plane standing-wave field arises from the superposition of two waves of equal wavelength and amplitude traveling in opposite directions. The interference between the waves results in the formation of parallel stationary planes of maximum velocity or pressure amplitude (antinode planes) and zero velocity or pressure amplitude (node planes). The node planes lie at half wavelength intervals, with the antinode planes lying equidistant between them. Pressure nodes coincide with velocity antinodes and *vice versa*. The ultrasonic forces on suspended particles result from the particle–fluid interactions that arise when the particles and suspending fluid have different acoustic properties (i.e., density and compressibility). The PRF is generated by the interaction of a particle with the primary wave field. The field reflected from a particle will generate a time-averaged SRF on an adjacent particle (Weiser et al., 1984).

Primary field forces

For compressible spherical particles suspended in an ideal fluid and small relative to the wavelength of the applied acoustic field, Gor'kov (1962) showed that the acoustic potential energy (U) of a single particle in a standing-wave field is given by

$$U = V_0\left[\frac{\beta_f - \beta_p}{\beta_f}\langle PE\rangle - \frac{3(\rho_p - \rho_f)}{\rho_f + 2\rho_p}\langle KE\rangle\right], \qquad (1)$$

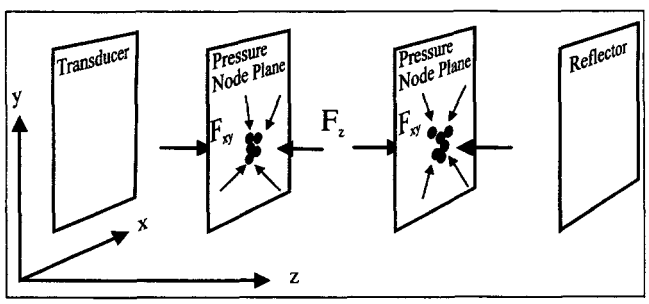

Figure 1. Particle aggregation by axial and transverse PRF in a nonuniform standing-wave field.

The sound propagates in the axial (z) direction. The E_{ac} of the field varies in the transverse (x,y) directions. The particles are driven by the axial primary radiation force (F_z) to the nearest pressure node plane (for $G > 0$). They then aggregate at the local E_{ac} maximum in the plane due to the transverse PRF (F_{xy}).

where β and ρ are, respectively, the compressibility and density of the particle (p) or fluid (f); V_0 is the static particle volume; $\langle PE\rangle$ and $\langle KE\rangle$ are the time-averaged potential and kinetic energy densities of the incident field, and can be expressed respectively as

$$\langle PE\rangle = \beta_f\langle p_{in}^2\rangle/2 \qquad (2)$$

and

$$\langle KE\rangle = \rho_f\langle |v_{in}^2|\rangle/2. \qquad (3)$$

For a standing-wave field with a nonuniform amplitude in the transverse directions x and y, the incident primary field pressure, p_{in}, and the first-order incident fluid velocity vector, v_{in}, are, respectively,

$$p_{in}(x,y,z,t) = p_0(x,y)\sin(\kappa z)\sin(\omega t) \qquad (4)$$

and

$$v_{in}(x,y,z,t) = v_0(x,y)\cos(\kappa z)\cos(\omega t)\boldsymbol{k}, \qquad (5)$$

where p_0 and $v_0 = p_0/\rho_f c$ are the x- and y-dependent pressure and velocity amplitudes; c is the sound speed in the liquid; $\kappa = 2\pi/\lambda$ is the wave number of the ultrasonic radiation; λ is the wavelength; $\omega = 2\pi f$ is the angular frequency; z is the axial distance from a pressure node; and $\boldsymbol{k}$ is the unit vector in the axial direction. The pressure and velocity amplitudes p_0 and v_0 were assumed to be constant in the axial direction. This idealization of the actual three-dimensional character of the field is considered further in the Discussion section.

Since $\boldsymbol{F} = -\nabla U$, Eqs. 1–5 can be combined to obtain the following expression for the axial component of the PRF:

$$F_z = -V_0 E_{ac}\kappa G\sin(2\kappa z)\boldsymbol{k}. \qquad (6)$$

The acoustic energy density, E_{ac}, is equal to the sum of the time-averaged potential and kinetic energy densities (Eqs. 2 and 3). The acoustic contrast factor, G, is given by

$$G = \left(\frac{\beta_f - \beta_p}{\beta_f} + \frac{3(\rho_p - \rho_f)}{\rho_f + 2\rho_p}\right). \qquad (7)$$

Equations 6 and 7 reduce to the expression derived by King (1934) for incompressible spheres, and are equivalent to that of Yosioka and Kawasima (1955) for compressible spheres. Particles such as mammalian cells in culture medium, for which $G > 0$, collect at the pressure-node planes (as shown in Figure 1), while bubbles in a liquid collect at the pressure antinode planes.

An expression for the transverse component of the PRF on a single particle in a pseudo-standing-wave field with a radially symmetric energy distribution was derived by Whitworth et al. (1991). For the more general field presented here, where the pressure amplitude is $p_0(x,y)$, the transverse force is found to be

$$F_{xy} = V_0 \nabla E_{ac} \left(\frac{3(\rho_p - \rho_f)}{\rho_f + 2\rho_p} \cos^2(\kappa z) - \frac{\beta_f - \beta_p}{\beta_f} \sin^2(\kappa z) \right). \quad (8)$$

The transverse PRF causes relatively incompressible particles suspended in a less dense medium to aggregate at the local E_{ac} maxima in the pressure nodes (Figure 1).

Secondary field force

For uniform acoustic fields, expressions for the SRF between two particles in an ideal fluid have been derived for incompressible spheres (Weiser et al., 1984) and compressible spheres (Crum, 1975; Weiser et al., 1984). For the case of two particles aligned parallel to the node planes, the SRF acting in the direction of the center-to-center line is expressed as

$$F_S = -\frac{E_{ac} V_0^2}{\pi l^2} \left[\frac{3(\rho_p/\rho_f - 1)^2 \sin^2(\kappa x)}{2l^2} + \kappa(1 - \beta_p/\beta_f)^2 \cos^2(\kappa x) \right], \quad (9)$$

where l is the center-to-center interparticle distance (Weiser et al., 1984). The force is attractive when $F_S < 0$. The particles are in contact when l equals two particle radii. Figure 2 compares the magnitude of the axial PRF on a single polystyrene bead (radius, $r = 5.1$ μm) to the attractive SRF between two such beads aligned parallel to the node planes with centers separated by a distance, l, as a function of axial distance from the pressure antinode plane ($E_{ac} = 18$ J/m^3, $f = 2.23$ MHz). The distance from the pressure antinode to the pressure node is 168 μm. The SRF is a maximum when the particles are in contact on the pressure-node plane ($l =$ 10.2 μm) and decreases rapidly with increasing interparticle distance. The maximum SRF is approximately two orders of magnitude weaker than the maximum axial PRF.

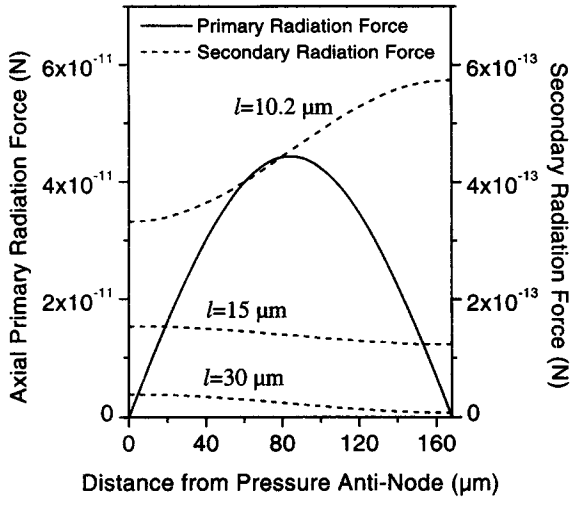

Figure 2. Magnitudes of axial PRF and SRF on 10.2-μm-dia. polystyrene particles for $E_{ac} = 18$ J/m^3, $f = 2.230$ MHz.

The PRF (left ordinate) and SRF (right ordinate) are plotted as functions of distance from the velocity node. The scale of the right ordinate is 100-fold lower than that of the left ordinate. The SRF is shown for three different interparticle distances (l). The SRF is strongest when particles are in contact ($l = 10.2\,\mu$m) and decreases rapidly with increasing l.

Effect of viscosity

Doinikov (1994) has shown that the viscosity of the suspending fluid can have a considerable influence on the primary radiation force. However, he demonstrated that using the ideal fluid approximation provides valid estimates of the PRF in cases where the particle radius is much smaller than the wavelength ($r \ll \lambda$) and much greater than the viscous boundary layer thickness ($r \gg (2\omega/\rho_f\mu)^{1/2}$). This case applies to the experimental conditions employed here ($r = 5.1 \times 10^{-6}$ μm, $\lambda/2\pi = 1.1 \times 10^{-4}$ μm, $(2\omega/\rho_f\mu)^{1/2} = 3 \times 10^{-7}$ μm), which are typical of the conditions used for mammalian cell separations. Thus, the expressions developed in the previous sections should yield good estimates of the PRF.

Acoustic energy density

The acoustic energy density, E_{ac}, is a measure of the energy residing in a wave field. In systems operated with nonresonant standing waves, a common technique for estimating the E_{ac} is to equilibrate the gravitational force with the PRF on particles with known acoustic properties (Weiser et al., 1984). For these systems the E_{ac} is proportional to the driving voltage. In a resonant system, such as the one used here, this method is not accurate. The proximity of the driving frequency to a resonance frequency strongly influences the E_{ac}. At the resonance frequency, the admittance (which is the inverse of the impedance) of the system reaches a maximum while the current and therefore the power density, P, to the system reach a peak for a constant driving voltage.

The degree of resonance in an oscillatory system can be characterized by quality factor, Q (French, 1971), defined as

$$Q = \frac{E_{ac}\omega}{P}. \quad (10)$$

Resonators driven at a resonance frequency with a high Q require a lower power input to generate a given E_{ac}. This minimizes temperature gradients and convective flows due to inhomogeneous heating of the resonator.

Principle of Ultrasonic Force Measurement

The force measurement system was developed based on the assumption that the observed particle velocities in a standing-wave field were proportional to the applied ultrasonic forces. In the absence of an acoustic field, suspended particles are subject to the gravitational force, fluid dynamic drag forces, and interparticle forces such as double-layer and hydrodynamic interactions. In the presence of a standing-wave field the particles are also subject to the PRF and the SRF. Forces tending to concentrate the particles are opposed by Brownian motion.

In the experimental system, the volume fraction of particles was less than 0.01% of 10.2-μm-diameter polystyrene beads in water. For such dilute conditions the average l is greater than 150 μm. For particles collected at the pressure node planes by the axial PRF, the average l is greater than 100 μm. Double-layer and hydrodynamic interactions are short-range forces relative to the separation distances involved in such a dilute particle system and may be neglected. The double-layer thickness in pure water (pH 7.0) is less than 1 μm and less than 10 nm for a 1-mM NaCl solution (Israelachvili, 1992). Hydrodynamically hindered sedimentation, or in this case hindered aggregation, becomes significant only at particle volume fractions greater than 10% (Zenz and Othmer, 1960). The SRF is calculated to be approximately six orders of magnitude lower than the axial PRF for $l = 100$ μm, and is therefore negligible for highly dispersed particles. The SRF may become significant relative to the transverse PRF under experimental conditions, as the particles aggregate near the local E_{ac} maximum. Diffusion due to Brownian motion may be neglected for 10-μm-diameter polystyrene particles in water (Zenz and Othmer, 1960).

When diffusion, the SRF, and double-layer and hydrodynamic interactions are neglected, the rate of change of particle momentum becomes equal to the sum of the ultrasonic forces $\boldsymbol{F}_z$ and $\boldsymbol{F}_{xy}$, the gravitational force, and the fluid drag force, $\boldsymbol{F}_D$, that is,

$$\left(\rho_p V_0 + \frac{\rho_f V_0}{2}\right)\frac{d\boldsymbol{v}}{dt} = \boldsymbol{F}_z + \boldsymbol{F}_{xy} + V_0(\rho_p - \rho_f)\boldsymbol{g} + \boldsymbol{F}_D, \quad (11)$$

where $\boldsymbol{v}$ is the particle velocity and $\boldsymbol{g}$ is the gravitational acceleration vector. The mass in the momentum change term is the "virtual mass" of the particle, that is, the sum of the true particle mass and a fluid mass that behaves effectively as if it were entrained with the particle. The maximum velocity for polystyrene particles in water due to the PRF under experimental conditions was of the order of 1 mm/s; yielding a Reynolds number of less than 0.01. The drag force is therefore given by Stokes' law, that is,

$$\boldsymbol{F}_D = -6\pi\mu r\boldsymbol{v}. \quad (12)$$

An analysis of the acceleration time demonstrates that for 10.2-μm polystyrene particles in water, the changes in particle and fluid momentum are negligible. The terminal velocity, v_∞, of an accelerating particle is reached when $dv/dt = 0$. From Eq. 11, the particle velocity as a function of time may be determined relative to the terminal velocity. Assuming a constant total ultrasonic force and a negligible gravity force, and setting $v = 0$ at $t = 0$, it is easily shown that

$$\frac{v}{v_\infty} = 1 - \exp\left[\frac{-6\pi\mu r}{(\rho_p + \rho_f/2)V_0}t\right]. \quad (13)$$

From Eq. 13, the time taken for a particle to reach 99% of terminal, its velocity was less than 4×10^{-2} ms, independent of the applied ultrasonic force. Displacements were measured experimentally at a minimum of 33-ms intervals. The transient is therefore negligible and the acceleration term may be eliminated from Eq. 11. The gravitational force was neglected in the axial PRF measurements because it acts normal to this force component under the experimental conditions employed. These considerations lead to the following direct relationship between the axial PRF and Stokes's drag:

$$\boldsymbol{F}_z = 6\pi\mu r v_z \boldsymbol{k}, \quad (14)$$

where v_z is the axial component of the particle velocity.

The transverse component of the PRF only has a detectable effect on the motion of particles once they collect in the nodal planes. Since the force of gravity acts parallel to the nodal planes, it must be included in the transverse PRF relation, that is,

$$\boldsymbol{F}_{xy} = 6\pi\mu r\boldsymbol{v} - V_0(\rho_p - \rho_f)\boldsymbol{g}. \quad (15)$$

The axial and transverse components of the PRF on a particle can thus be determined independently; the axial component is determined from the measured axial particle velocities, and the transverse component from the transverse velocities of particles in the pressure-node planes.

Experimental Apparatus

An exploded view of the ultrasonic resonance chamber is shown in Figure 3. The composite transducer (SonoSep Biotech Inc., Richmond, BC, Canada) consisted of a 1-mm-thick 2.5-cm^2 PZT piezoelectric ceramic with a fundamental frequency of 2 MHz bonded to 2.2-mm-thick borosilicate glass. The reflector was a single piece of the same glass. The transducer and reflector were held in place by clamps and sealed with silicone gaskets. The body of the chamber was constructed of stainless steel. The distance between the transducer side and reflector side of the chamber was 29.30 mm $\pm$ 0.01 mm. Parallel surfaces were required to ensure a high quality factor resonance. Windows machined on three sides were fitted with 1.7-mm-thick borosilicate glass to permit microscopic imaging. Polystyrene particle suspensions were added through the opening on top of the chamber.

Polystyrene microspheres (Seradyn, Indianapolis, IN) were employed as model particles for the experimental investigations. The microspheres have known uniform acoustic properties similar to those of mammalian cells and are highly uniform in diameter. They were suspended in distilled water. The pertinent properties of the microspheres and the suspending medium are listed in Table 1.

The force-measurement apparatus is depicted in Figure 4. Particle motion in the resonator chamber was monitored through the windows of the chamber with an inverted micro-

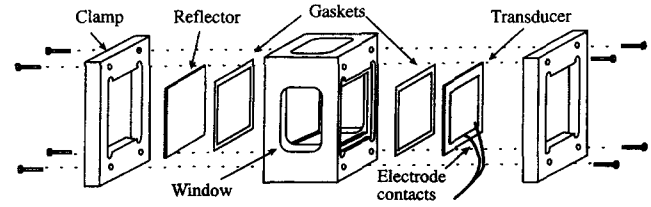

Figure 3. Acoustic chamber construction.
The reflector and transducer are held by clamps and sealed by silicone rubber gaskets.

Table 1. Physical Properties of Polystyrene Latex Particles and Degassed Distilled Water at 25°C, 1 atm

	Polystyrene Latex	Degassed Distilled Water
Density (g/mL)	1.053*	0.997†
Sound speed (compression) (m/s)	—	1,497††
Adiabatic compressibility (Pa^{-1})	2.16×10^{-10}**	4.48×10^{-10}**
Particle diameter (μm)	10.20 ± 0.09	—
Viscosity (Pa·s)	—	9.98×10^{-4}†

* Javanaud and Anson, 1989.
** Hay and Burling, 1982.
† Weast et al., 1986.
†† McSkimin, 1965.

scope (Wild Heerbrugg, Germany) and recorded on video (Sony SLV-380, Japan) via a CCD camera (COHU, San Diego, CA). The chamber was attached to a stage whose position could be controlled in three dimensions by micromanipulators accurate to ±0.05 mm (Brinkmann, Germany). A removable needle projecting into the chamber through its top opening was used to set reference coordinates for the micromanipulators. For axial PRF measurements in the y-z plane (as defined in Figure 1), particles were imaged by transmitted light through the side windows. For transverse PRF measurements in the x-y plane, reflected light was employed to image the particles through the reflector.

A computer-controlled admittance measurement device was employed for off-line quality factor determination (Schmid et al., 1990). The series resonance frequency (f) is at the electrical conductance (or real part of the admittance) peak. For an undistorted conductance spectrum (Figure 5) the quality factor may be calculated from

$$Q=\frac{f_{+1/2}+f_{-1/2}}{2(f_{+1/2}-f_{-1/2})}, \tag{16}$$

where $f_{+1/2}$ and $f_{-1/2}$ are the frequencies at the half-peak height. Experiments were performed in the frequency range between 2.1 and 2.4 MHz, where the quality factor, Q, of the resonator reached a plateau.

The piezoceramic transducer was driven by an electronic power supply developed for ultrasonic separation applications that allowed on-line measurement of the power input to the resonator (SonoSep Biotech Inc. USCS-04, Richmond,

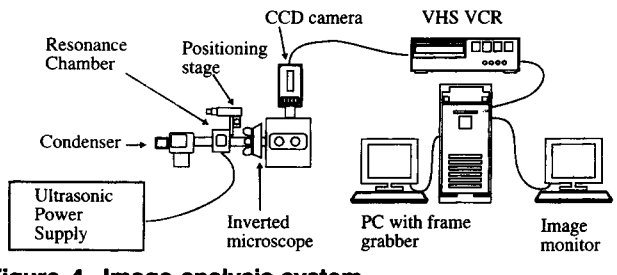

Figure 4. Image analysis system.

Images of particle motion in the resonator chamber are acquired through a microscope equipped with a CCD camera. The images are stored on a VCR and subsequently digitized.

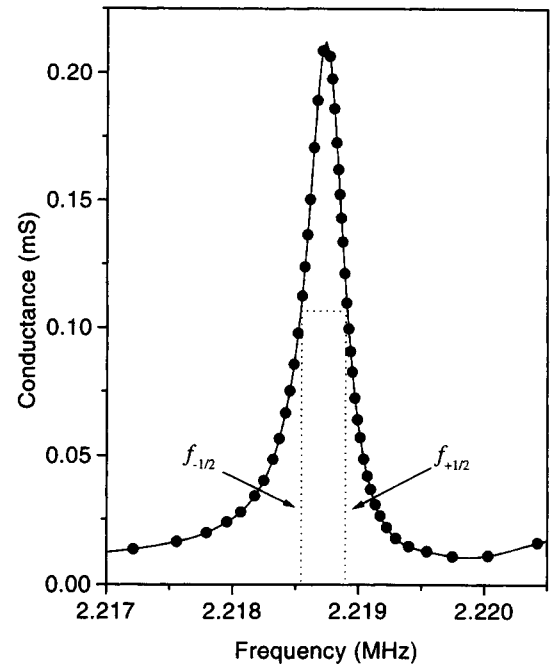

Figure 5. Conductance as a function of frequency for the ultrasonic chamber filled with air-saturated distilled water at 23°C.

The quality factor, Q, of the resonator may be calculated at each resonance frequency from the characteristic frequencies $f_{-1/2}$ and $f_{+1/2}$ of the conductance spectrum (Eq. 16). For this resonance frequency $f = 2.2187$ MHz, $Q = 5{,}600$.

BC, Canada). For the force measurements, the frequency was set to the resonance peak nearest 2.23 MHz by maximizing the input power at constant voltage (see the Background and Acoustic Energy Density sections). The particles were dispersed in distilled water with a pipette and transient bulk flows were allowed to attenuate for approximately 2 min before reapplying the field and recording the particle trajectories. By running the power supply continuously and switching from a dummy load to the resonator, transients in power amplification were avoided that otherwise would have arisen during the powering-up period.

To obtain the calculated E_{ac} values (Eq. 10), it was assumed that all the power dissipation occurred in the liquid. In reality, power is also dissipated in the reflector and transducer, which together represent 18% of the active resonator volume. However, the design and operation of the resonator were such that more than 95% of the power dissipation was predicted to occur in the liquid (Gröschl, 1997). The initial assumption is therefore appropriate.

In the case of the transverse PRF measurements, convective flows due to acoustic streaming and heating in the unrestricted chamber volume were more disruptive, due to the relatively lower induced particle velocities (approximately 10 μm/s vs. 1 mm/s for the axial measurements). To limit these flows, the free-water volume in the chamber was reduced by more than 95% by casting a 4% polyacrilamide gel in the chamber (gel: 18 mL distilled water, 2 mL 40% polyacrilamide, 20 μL tetramethylethylenediamine, 160 μL ammonium persulfate; Biorad, Hercules, CA). The gel was cast around a mold with three vertical legs. The resulting gel,

viewed through the upper opening of the chamber, had one open central column with a 0.5-by-0.5-cm cross section. This was the measurement volume. The other two columns (1.0 by 0.5 cm) were offset on either side of the central column such that the sound travel time was equivalent for all axial paths in the resonator, and conditions for resonance in the chamber were maintained. The gel did not perceptibly affect the shape of the admittance spectrum. However, the quality factor was approximately 30% lower than for distilled water due to increased attenuation.

Sequential images were acquired from the computer-controlled VCR by a frame grabber (Coreco Oculus TCX, St. Laurent, PQ, Canada) at a minimum time interval of 1/30 s and stored on a 90-MHz Pentium PC. Image analysis was performed using Optimas 4.0 utilities and macros (Bioscan, Bothell, WA). The image plane dimensions were calibrated using a precision etched glass slide (Fuch Rosenthal, Hausser Scientific, Horsham, PA). Particles were resolved from the background of the digitized images using a modified 9×9 Mexican hat filter (Lee et al., 1994) that combines edge detection and smoothing in one operation. The single particles were distinguished from noise, doublets, and larger aggregates by satisfying two morphological criteria: $50 < \text{area} < 200$ μm^2 and circularity < 18. Circularity is defined as the ratio of the squared circumference to the area. It has a minimum value of 12.57 (4π) for a circle. Particle positions were calculated from the two-dimensional "center of mass" of the pixels defining each particle area. Particle displacements from frame to frame were determined using a modified nearest-neighbors algorithm (Noble and Levine, 1986). The algorithm identified all the particles in the image that were within a given distance of each particle in the previous image. Unambiguously matched particles were paired on the first pass and the process was repeated with the remaining particles until no more unambiguous matches could be made. For the axial PRF measurements an elliptical search area with the long axis in the axial direction was used for improved discrimination between neighboring particles.

The particle velocities were calculated from the displacement and the time interval between frames. The corresponding particle position was the average of the initial and final positions. For the axial PRF measurements, the error due to the assumption of constant velocity during each time interval is less than 5% for particles more than 16 μm from the nodal plane (5% of the internodal distance). Particle displacements due to the transverse PRF are even weaker functions of position; therefore the constant velocity assumption is appropriate. The field can be assumed to be at full strength the instant that power is applied. The time taken for the acoustic field to reach 99% of maximum E_{ac} was approximately 1.6 ms ($Q = 5{,}000$, $f = 2.23$ MHz) compared to the 33-ms time-interval between successive captured images.

Experimental Results

A typical sequence of images acquired in the y-z plane shows randomly dispersed polystyrene particles (Figure 6, $t = 0$ s) being driven to the pressure-node planes of the ultrasonic resonance field by the axial PRF (Figure 6, $t = 0.1$–0.3 s). The time interval between the frames was 0.1 s. The pressure node planes coincide with the particles aligned in the

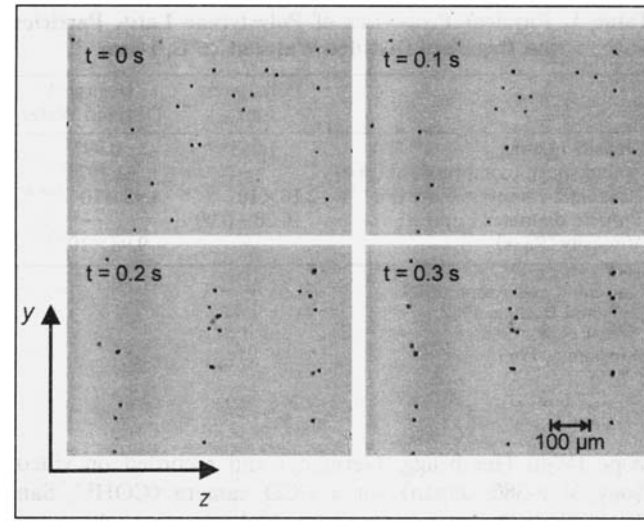

Figure 6. Displacement of polystyrene microspheres by the axial PRF.

The axial displacement of particles is shown between successive images at 0.1-s time intervals. The plane of image capture was parallel to the direction of sound propagation.

y-direction at $t = 0.3$ s in Figure 6. In this sequence the particle reached a maximum velocity of 750 μm/s for an input power of 26 W/L.

The axial PRF on the particles was calculated from their measured velocities using Eq. 14. In Figure 7 the measured particle velocity (left ordinate) and calculated axial PRF (right ordinate) are plotted as a function of the axial position in the field. The data were determined from the trajectories of the 21 particles in the field of view of Figure 6 and were obtained in a region near the center of the resonance chamber. A positive axial velocity indicates displacement toward the transducer. The axial PRF fell to zero at the pressure and velocity

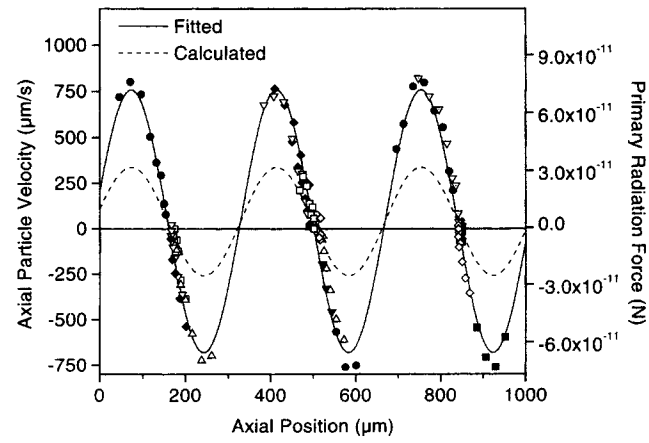

Figure 7. Particle velocity (left) and axial PRF (right) as a function of axial position ($f = 2.230$ MHz, $P = 26$ W/L, $Q = 5{,}600$).

Different symbols represent the velocity profiles of individual particles. The best fit of the data with curve $F_z = A\sin(2\kappa(z-\phi)) + B$ (solid line) is found for $A = 6.9\times10^{-11}$ N, $\kappa = 0.00923$ μm^{-1}, $\phi = -12.6$ μm, and $B = 3.8\times10^{-12}$ N. The calculated average velocity amplitude for the chamber was 2.9×10^{-11} N (dashed line).

node planes and the particles collected at the pressure-node planes. This figure demonstrates clearly that the axial PRF follows the sinusoidal variation with position predicted by Eq. 6.

A nonlinear least-squares fit of the axial PRF data was performed using the Levenberg-Marquardt routine (Press et al., 1992). The fitting model $F(z) = A\sin[2\kappa(z-\phi)]+B$ was based on Eq. 6, modified to include a phase shift, ϕ, and an offset, B. The constant A replaces the product $V_0 E_{ac}\kappa G$, where E_{ac} was assumed to be constant within the image region. The phase shift accounted for the arbitrary origin of the acquired data. The offset, B, quantified the magnitude of bulk fluid flows existing at the time of the measurement. B was treated as a constant for the fitting procedure, even though it decreases as a function of time. Only experimental data for which B was less than 10% of A were retained. This procedure minimized the distortion of the measured particle velocities due to the progressive attenuation of the axial bulk flows by particles collecting at the pressure-node planes.

The wavelength estimated using the fitted model was 681 μm; the value calculated from the sound speed and frequency was 671 μm. The wavelength from the first fitting step was fixed and a second fitting step was performed in which A was recalculated using a data set reduced to include only those points whose amplitude was greater than 20% of the initial A value. This procedure ensured that the large number of data points near the nodes where measurement uncertainty is highest did not affect the calculation of A. An effective $E_{ac} = 24$ J/m^3 was calculated from the fitted axial PRF amplitude and the parameters in Table 1. This compared to $E_{ac} = 10.3$ J/m^3 calculated from the measured power, resonance frequency and quality factor. The large discrepancy between the calculated and the fitted values of E_{ac} is likely due to the nonuniform energy distribution in the field and is addressed later in this section.

Despite the nonuniform energy density of the field, the relationship between the power, P, and the axial PRF is expected to be linear at any given resonance frequency and location in the field due to the linear dependence of the axial PRF on E_{ac} (Eq. 6). To demonstrate this linear relationship, experiments were performed at another central location in the field for powers of approximately 30 and 55 W/L. The fitted axial PRF amplitudes were determined as described earlier and are shown in Figure 8. The best straight-line fit through the origin predicted a local E_{ac}/P ratio of 3.1×10^{-4} J/W (based on the physical properties in Table 1). For the measured quality factor of 4,000, the calculated average E_{ac}/P was 2.85×10^{-4} J/W. The discrepancy between fitted and calculated values is only 10% in this case.

The fitted E_{ac} values were the averages for the 0.7×1.0-mm measurement area only, whereas the calculated E_{ac} values represent average values for the whole chamber (2.5 cm on each side). Measurements performed at the center of the resonator, such as those in Figures 7 and 8, demonstrated that the fitted E_{ac} values were higher than the calculated averages. However, measurements performed near the sidewalls yielded fitted E_{ac} values close to zero. In addition to this longer-range variation between the center and sidewalls, a local variability in E_{ac} of as much as twofold was also observed over distances of 1 to 2 mm in the central region at constant Q and P. These local and long-range variations explain the discrepancies between the fitted and calculated values of the E_{ac} in Figures 7 and 8.

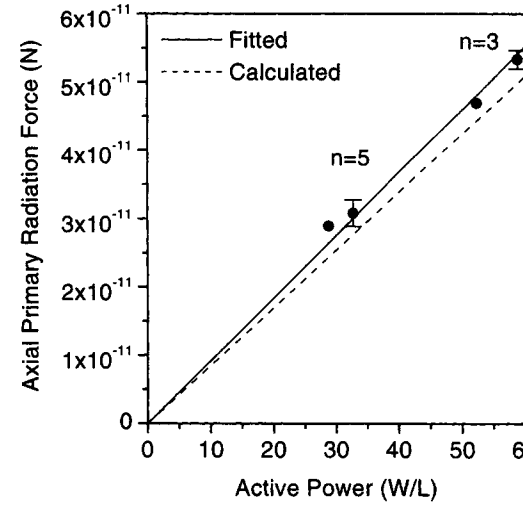

Figure 8. Axial PRF as a function of input power at a particular location in the ultrasonic chamber.

Error bars accompanying the points with $n = 5$ and $n = 3$ replicates show the 95% c.i. for the mean. The best-fit line through the origin (solid line) corresponds to $E_{ac}/P = 3.1\times10^{-4}$ J/W. The dotted line shows the slope corresponding to the calculated average E_{ac}/P ratio of 2.85×10^{-4} J/W (Q = 4,000, f = 2.232 MHz).

Quantification of the E_{ac} variation within the resonator cross section is of great interest because it is responsible for particle aggregation by the transverse PRF. The local transverse E_{ac} variation should manifest itself in the y-z image plane as a distinct trend in the axial PRF amplitude with transverse position y. In order to detect this transverse variation in the axial PRF, the microscope was focused on a region where an aggregate was observed to form within 30 s of sonication. The values of κ, ϕ, and B were obtained from the fit of the model $F(z) = A\sin[2\kappa(z-\phi)]+B$ to all the data, and then the maximum force on individual particles was determined by finding the values of A that gave the best fit of the individual particle data. Only trajectories having more than three data points, with at least one point near an axial force maximum [i.e., $\sin(z-\phi) > 0.95$] were analyzed. This requirement eliminated data sets having no useful information about the axial force amplitude.

The variation in the axial PRF with transverse particle position in the resonance field is plotted in Figure 9 for four data sets collected at each of $P = 24$ W/m^3 and $P = 46$ W/m^3. There was a linear trend of decreasing axial PRF with increasing transverse position at both the low and high power levels, with a statistically significant slope ($p < 0.01$). The observed scatter may be explained in part by the fact that, despite the relatively narrow focal plane of the order of 12.5 μm (lens N.A. = 0.1), particles within $x = \pm100$ μm of the y-z plane were imaged due to their occlusion of the light collected at the lens. Therefore, at any given transverse y point in the image, there is a variability in the observed E_{ac} due to the additional out-of-plane (x) dependence of the E_{ac}.

The E_{ac} gradient in the transverse y-direction was calculated from the slope of the line of best fit for each set of data, and the transverse PRF (on a 10.2-μm-dia. polystyrene

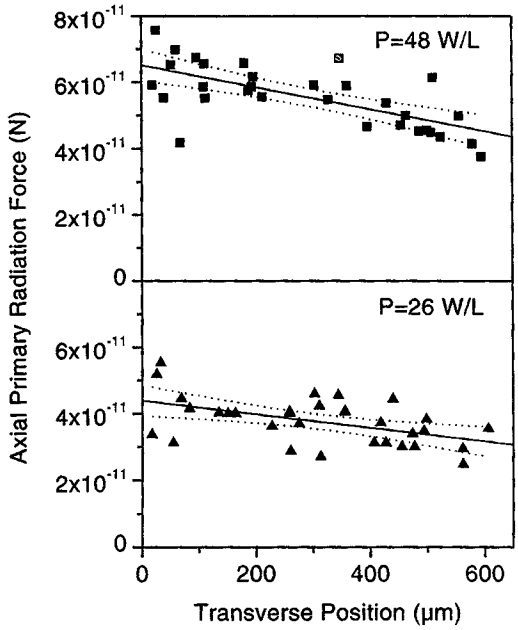

Figure 9. Axial PRF as a function of transverse particle position.

The axial PRF amplitudes of individual particles pooled for $n = 4$ data sets at $P = 48$ W/m^3 and $P = 26$ W/m^3 demonstrate a statistically significant ($p < 0.01$) dependence on particle position. The 95% c.i. for the fits appear as dotted lines.

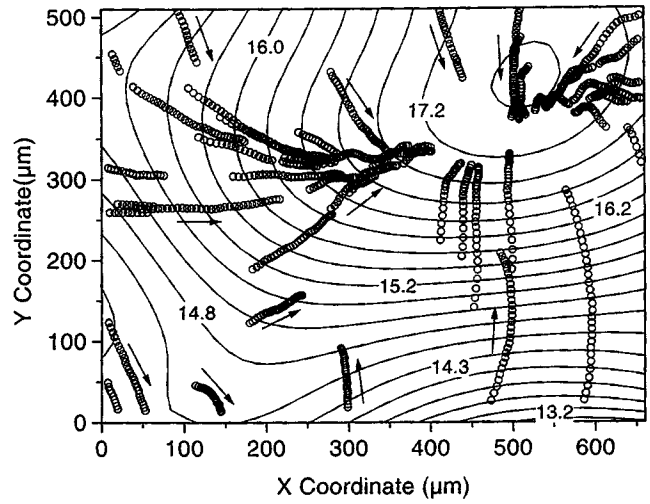

Figure 10. Particle displacement in a transverse pressure-node plane due to the transverse PRF.

The particles (open circles) are shown converging within the pressure-node plane. Arrows indicate the direction of particle motion. The E_{ac} distribution (solid contour lines) was determined by fitting the x and y components of the gradient of a sixth-order polynomial describing E_{ac} to the components of the transverse PRF (Eq. 8). The contour levels are expressed in J/m^3.

sphere) was estimated using Eq. 8. The results, summarized in Table 2, show that the estimated transverse PRF was two orders of magnitude less than the axial PRF. The assumption of constant E_{ac} in the axial direction is also supported by these results. The gradients in the E_{ac} measured here are negligible relative to the gradients in the kinetic and potential energy that give rise to the force in Eq. 6. Therefore, the additional axial force due to the E_{ac} gradients is negligible.

The approximate proportionality observed between the estimated ∇E_{ac} and P implies that the E_{ac} ratio between any two transverse locations is invariant with P for a given resonance frequency. Under these circumstances, the ∇E_{ac} and the transverse PRF are linear functions of P, as are the axial PRF and SRF.

Direct measurements of the transverse PRF were performed by focusing the microscope on a pressure-node plane at an aggregation site near the center of the chamber. In Figure 10 particle positions measured at 1-s intervals, with $P =$ 59 W/L, are represented by converging open circles. The measured particle velocities were about 10 μm/s. A gel restricted the free-fluid volume in the resonator, minimizing convective fluid flows sufficiently that their effect on particle aggregation was undetectable (see the Experimental Apparatus section).

Table 2. Estimate of the Transverse PRF on a 10-μm-dia. Polystyrene Particle as a Function of Power for $Q = 5600$

Input Power (W/L)	Transverse PRF (N)	Avg. Axial PRF Amplitude (N)
24	2.0×10^{-13}	3.8×10^{-11}
46	3.2×10^{-13}	5.6×10^{-11}

Under the present experimental conditions, the predicted SRF between two polystyrene particles in contact at the pressure-node plane is of the same order as the transverse PRF. However, at a center-to-center interparticle distance of $l = 20$ μm, the SRF is calculated to be 10-fold lower than the transverse PRF, and 100-fold lower at $l = 35$ μm. The following restrictions were established to ensure that the SRF had a negligible impact on the transverse PRF calculations: (1) each particle trajectory was acquired only while the nearest neighbor was more than 20 μm distant; and (2) analysis of the aggregation sequences was halted when more than 10% of the particles had a nearest neighbor within 35 μm.

The transverse PRF on each particle as a function of its position was determined from Eq. 15. The x and y components of the E_{ac} gradient were then calculated from Eq. 8. An nth order polynomial in x and y was used to describe the E_{ac} distribution in the image region. The coefficients of the polynomial were determined by minimizing simultaneously the sum of squared differences between the x and y components of the polynomial gradient and the calculated E_{ac} gradient data. The fit was assessed by evaluating $r^2 = (1-$ SSR)/SST, where SSR is the sum of squares of the residuals and SST is the total sum of squares. The fit improved from $r^2 = 0.50$ to 0.82 as the order of the polynomial was increased from second to sixth order. A relative plateau was attained above sixth order. The fitted 6th-order polynomial of the E_{ac} distribution is plotted in Figure 10 as solid contour lines with levels marked in J/m^3. Due to the additional influence of gravity, some particle trajectories are not perpendicular to the contour lines and the point of maximum E_{ac} is above the aggregation point.

The average and peak transverse PRF magnitudes were calculated from the fitted E_{ac} distribution. The border areas (10% of the total area) at the edges of the image were omit-

Table 3. Average and Peak Transverse PRF Magnitudes Calculated from the E_{ac} Distribution

Power (W/L)	Avg. Transverse PRF (N)	Peak Transverse PRF (N)
59	2.3×10^{-13}	4.4×10^{-13}
69	2.9×10^{-13}	5.4×10^{-13}

ted in this analysis due to the unreliability of the polynomial fit in those regions. The average and peak transverse PRF for the E_{ac} distribution in Figure 10 and those for a second experiment at this identical field location and resonance frequency, but with $P = 69$ W/L, are shown in Table 3. There is good agreement on the magnitude of the transverse PRF as a function of input power between the estimates based on the smoothed E_{ac} distribution (Table 3) and those based on the axial PRF variation (Table 2).

Concluding Remarks

The operating power level in a mammalian-cell separation resonator for perfusion bioreactors is typically an order of magnitude higher ($P = 750$ W/L) than in the experimental system described here. Extrapolating linearly with power level, the transverse PRF would be approximately 6×10^{-12} N, 20 times greater than the gravitational force on a single particle (3×10^{-13} N). The approximate flow rate against which a single 10.2-μm-dia. particle could be held by the transverse PRF at these power levels is 60 μm/s. Under similar operating conditions single particles could be retained by the axial PRF against flow velocities of the order of 1 cm/s.

Taking these observations in isolation, it would appear that exploitation of the axial PRF is the logical choice for particle–liquid separation. Flowthrough systems based solely on the axial force generally operate by transporting and concentrating particles in one region of the separator (Benes et al., 1991; Whitworth et al., 1991; Frank et al., 1993), thereby requiring a net fluid flow through the nodal planes. Particles collecting on the nodal planes obstruct the flow cross section, increasing the effective fluid velocity and the fluid drag on the particles. A particle concentration of 3% v/v of 10-μm particles in a separator operated at 2 MHz would result in particle monolayers instantly filling the pressure-node planes. Such systems may thus be more effective for separating dilute suspensions.

In separation systems exploiting the transverse PRF for particle retention, fluid flow is parallel to the nodal planes where the particles collect due to the axial force. Trampler et al. (1994) have shown that the transverse PRF can retain greater than 90% of the particles in high-concentration suspensions (over 5% v/v) for superficial velocities up to 1.3 mm/s, a velocity 20 times the estimated maximum for retention of a single particle. The increase in maximum flow velocity likely occurs because cells are retained primarily as aggregates in the flowthrough system, where the total ultrasonic and gravitational forces retaining the aggregates increase as a function of aggregate volume, while the drag force increases as a function of the exposed surface area.

The axial and transverse primary radiation force measurements have not only served to clarify the mechanism of ultrasonic cell separation, but have provided an understanding of the typical E_{ac} distribution in a resonator. Knowledge of the force distribution in the complete resonator is crucial to the development of predictive models of particle retention in real systems. Such models will assist in the evaluation of potential applications and appropriate operating strategies, accelerating the design of ultrasonic resonator-based separation systems.

Acknowledgments

One of the authors (S. M. W.) was supported by Natural Sciences and Engineering Research Council (NSERC) and BC Science Council GREAT Scholarships. This work was funded by NSERC, and the acoustic resonators and electronics were provided by SonoSep Biotech Inc. (Richmond, BC). We thank M. Gröschl and E. Benes at the Institut für Allgemeine Physik, Technische Universität Wien, Austria, and F. Trampler, S. Sonderhoff, and J. Poppleton at SonoSep Biotech Inc. for valuable discussions.

Notation

c = sound speed in fluid, m/s
E_{ac} = acoustic energy density, J/m^3
f = frequency, s^{-1}
F_S = secondary radiation force, N
F_{xy} = transverse primary radiation force, N
F_z = axial primary radiation force, N
G = acoustic contrast factor (Eq. 7), dimensionless
g = gravitational acceleration vector, m/s^2
i, j, k = unit vectors in x, y, and z-directions
KE = kinetic energy density, J/m^3
l = center to center interparticle distance, m
P = power density, W/m^3
p_0 = pressure amplitude of incident acoustic wave, Pa
PE = potential energy density, J/m^3
p_{in} = local pressure of incident acoustic wave, Pa
Q = quality factor, dimensionless
r = particle radius, m
t = time, s
v = velocity of particle, m/s
V_0 = volume of particle, m^3
v_{in} = local velocity of incident acoustic wave, m/s
v_0 = velocity amplitude of incident acoustic wave, m/s
v_z = axial component of particle velocity, m/s
x, y = transverse particle coordinates, m
z = axial particle coordinate, m
β = compressibility, Pa^{-1}
∇ = gradient operator: $(\partial/\partial x)\boldsymbol{i} + (\partial/\partial x)\boldsymbol{j} + (\partial/\partial x)\boldsymbol{k}$
λ = wavelength, m
κ = wave number (ω/c), m^{-1}
μ = fluid viscosity, Pa·s
ρ = density, kg/m^3
ω = angular frequency ($2\pi f$), s^{-1}

Subscripts

f = fluid
p = particle

Literature Cited

Benes, E., F. Hager, W. Bolek, and M. Gröschl, "Separation of Dispersed Particles by Drifting Ultrasonic Resonance Fields," *Proc. Ultrason. Int. Conf.*, Le Touquet, France, Butterworth-Heinemann, Oxford, 167 (1991).

Crum, L. A., "Bjerknes Forces on Bubbles in a Stationary Sound Field," *J. Acoust. Soc. Amer.*, **57**(6i), 1363 (1975).

Doblhoff-Dier, O., Th. Gaida, H. Katinger, W. Burger, M. Gröschl, and E. Benes, "A Novel Ultrasonic Resonance Field Device for the Retention of Animal Cells," *Biotechnol. Prog.*, **10**, 428 (1994).

Doinikov, A. A., "Acoustic Radiation Pressure on a Compressible Sphere in a Viscous Fluid," *J. Fluid Mech.*, **267**, 1 (1994).

Frank, A., W. Bolek, M. Gröschl, W. Burger, and E. Benes, "Separation of Suspended Particles by Use of the Inclined Resonator

Concept," *Proc. Ultrason. Int. Conf.*, Vienna, Austria, Butterworth-Heinemann, Oxford, 519 (1993).
French, A. P., *Vibrations and Waves*, Norton, New York (1971).
Gor'kov, L. P., "On the Forces Acting on a Small Particle in an Acoustical Field in an Ideal Fluid," *Sov. Phys. Dokl.*, **6**(9), 773 (1962).
Gröschl, M., "Ultrasonic Separation of Suspended Particles: I. Fundamentals, *Acustica*, in press (1997).
Gupta, S., D. L. Feke, and I. Manas-Zloczower, "Fractionation of Mixed Particulate Solids According to Compressibility Using Ultrasonic Standing Wave Fields," *Chem. Eng. Sci.*, **50**(20), 3275 (1995).
Hay, A. E., and R. W. Burling, "On Sound Scattering and Attenuation in Suspensions, with Marine Applications," *J. Acoust. Soc. Amer.*, **72**(3), 950 (1982).
Higashitani, K., M. Fukushima, and Y. Matsuno, "Migration of Suspended Particles in Plane Stationary Ultrasonic Field," *Chem. Eng. Sci.*, **36**(12), 1877 (1981).
Israelachvili, J. N., *Intermolecular and Surface Forces*, 2nd ed., Academic Press, London (1992).
Javanaud, C., and L. W. Anson, "Reinterpretation of Ultrasonic Velocity Data on Polystyrene Latex Dispersions," *J. Phys. Chem.*, **93**, 499 (1989).
Johnson, D. A., and D. L. Feke, "Methodology for Fractionating Suspended Particles Using Ultrasonic Standing Wave and Divided Flow Fields," *Sep. Technol.*, **5**, 251 (1995).
King, L. V., "On the Acoustic Radiation Pressure on Spheres," *Proc. R. Soc.*, **a147**, 212 (1934).
Kundt, A., and O. Lehmann, "Longitudinal Vibrations and Acoustic Figures in Cylindrical Columns of Liquids," *Annal. Phys. Chem.*, **153**, 1 (1874).
Lee, Y., L. V. McIntire, and K. Zygourakis, "Analysis of Endothelial Cell Locomotion: Differential Effects of Motility and Contact Inhibition," *Biotechnol. Bioeng.*, **43**, 622 (1994).
Mandralis, Z. I., and D. L. Feke, "Continuous Suspension Fractionation Using Acoustic and Divided Flow Fields," *Chem. Eng. Sci.*, **48**(23), 3897 (1993a).
Mandralis, Z. I., and D. L. Feke, "Fractionation of Suspensions Using Synchronized Ultrasonic and Flow Fields," *AIChE J.*, **39**(2), 197 (1993b).
McSkimin, H. J., "Velocity of Sound in Distilled Water for the Temperature Range 20–75°C," *J. Acoust. Soc. Amer.*, **37**(2), 325 (1965).
Noble, P. B., and M. D. Levine, *Computer-assisted Analysis of Cell Locomotion and Chemotaxis*, CRC Press, Boca Raton, FL (1986).
Press, W. H., S. A. Teukolsky, W. T. Vetterling, and B. P. Flannery, *Numerical Recipes in C: The Art of Scientific Computing*, 2nd ed., Cambridge Univ. Press, Cambridge, England (1992).
Pui, P. W. S., F. Trampler, S. A. Sonderhoff, M. Gröschl, D. G. Kilburn, and J. M. Piret, "Batch and Semi-continuous Aggregation and Sedimentation of Hybridoma Cells by Acoustic Resonance Fields," *Biotechnol. Prog.*, **11**, 146 (1995).
Schmid, M., E. Benes, and R. Sedlaczek, "A Computer-controlled System for the Measurement of Complete Admittance Spectra of Piezoelectric Resonators," *Meas. Sci. Technol.*, **1**, 970 (1990).
Trampler, F., S. A. Sonderhoff, P. W. S. Pui, D. G. Kilburn, and J. M. Piret, "Acoustic Cell Filter for High Density Perfusion Culture of Hybridoma Cells," *Bio/Technology*, **12**, 281 (1994).
Weast, R. C., M. J. Astle, and W. H. Beyer, eds., *CRC Handbook of Chemistry and Physics*, CRC Press, Boca Raton, FL (1986).
Weiser, M. A. H., R. E. Apfel, and E. A. Neppiras, "Interparticle Forces on Red Cells in a Standing Wave Field," *Acoustica*, **56**, 114 (1984).
Whitworth, G., M. A. Grundy, and W. T. Coakley, "Transport and Harvesting of Suspended Particles Using Modulated Ultrasound," *Ultrasonics*, **29**, 439 (1991).
Whitworth, G., and W. T. Coakley, "Particle Column Formation in a Stationary Ultrasonic Field," *J. Acoust. Soc. Amer.*, **91**(1), 79 (1992).
Yosioka, K., and Y. Kawasima, "Acoustic Radiation Pressure on a Compressible Sphere," *Acustica*, **5**, 167 (1955).
Zenz, F. A., and D. F. Othmer, *Fluidization and Fluid-Particle Systems*, Reinhold, New York (1960).

Manuscript received Dec. 12, 1996, and revision received Mar. 4, 1997.